

1961

Angle Sensitivity of a Silicon Cell Solar Sensor Application of Electromagnetic Radiation Pressure for Plasma Acceleration

Theodore Morin
College of William & Mary - Arts & Sciences

Follow this and additional works at: <https://scholarworks.wm.edu/etd>



Part of the [Electromagnetics and Photonics Commons](#)

Recommended Citation

Morin, Theodore, "Angle Sensitivity of a Silicon Cell Solar Sensor Application of Electromagnetic Radiation Pressure for Plasma Acceleration" (1961). *Dissertations, Theses, and Masters Projects*. William & Mary. Paper 1539624524.

<https://dx.doi.org/doi:10.21220/s2-0na0-kw98>

This Thesis is brought to you for free and open access by the Theses, Dissertations, & Master Projects at W&M ScholarWorks. It has been accepted for inclusion in Dissertations, Theses, and Masters Projects by an authorized administrator of W&M ScholarWorks. For more information, please contact scholarworks@wm.edu.

APPLICATION OF ELECTROMAGNETIC
RADIATION PRESSURE FOR PLASMA
ACCELERATION

By

Theodore Morin, B.S.

A Thesis Presented to
The Faculty of the Department of Physics
College of William and Mary

In Partial Fulfillment
of the requirements for the Degree
Master of Arts

January 1961

APPLICATION OF ELECTROMAGNETIC
RADIATION PRESSURE FOR PLASMA
ACCELERATION

By Theodore Morin, B.S.

Williamsburg, Virginia

January 17, 1961

A thesis presented to the
Faculty of the Department of Physics
of the College of William and Mary
in Virginia in partial fulfillment
of the requirements for the degree of Master of Arts

Approved:

James D. Lawrence, Jr.
J. E. McManus

Frederic R. Tompfield, Jr.
Chm.

Jan 14, 1961

TABLE OF CONTENTS

CHAPTER	PAGE
I. INTRODUCTION	1
II. ACCELERATION OF A PLASMA BY RADIATION PRESSURE	3
Definition of a plasma	3
Force exerted on a reflecting surface by electro- magnetic radiation	3
III. PRODUCTION AND MEASUREMENT OF THE PLASMA	5
Radio frequency breakdown	5
Velocity measurements	7
IV. APPARATUS	8
Description of equipment used for producing the plasma .	8
Accelerator	9
Plasma detection equipment	9
Signal decay measurements	11
Total current output measurements	12
Vacuum system	12
V. INTERPRETATION OF DATA	14
Analysis of velocity measurements	14
Comparison of signal decay measurements	14
Effect of magnetic field on breakdown	16
Electromagnetic force on the plasma	17
VI. CONCLUSION	20
BIBLIOGRAPHY	38
APPENDICES	39
ACKNOWLEDGEMENTS	47

TABLE OF FIGURES

FIGURE	PAGE
1. Schematic of microwave circuit and method of making velocity measurements using photocells	21
2. Helmholtz coils	22
3. Entire experimental setup	23
4. Coaxial accelerator	24
5. Two Teflon "windows" and center conductor	25
6. Vacuum system	26
7. Velocity runs with photocells. Air at a pressure of 5μ Hg..	27
8. Velocity runs with photocells. Helium at a pressure of 5μ Hg.	28
9. Velocity runs with induction probe, air	29
10. Velocity runs with induction probe, helium	29
11. Comparison of light signal decay to induction probe signal decay as a function of distance from the accelerator, air .	30
12. Comparison of light signal decay to inductive probe signal decay as a function of distance from the accelerator, helium.	31
13. Light decay as a function of distance from accelerator. Air at a pressure of 5μ Hg	32
14. Light decay as a function of distance from the accelerator. Helium at a pressure of 5μ Hg	33
15. Inductive probe signal decay as a function of distance from the accelerator. Air at a pressure of 5μ Hg	34
16. Inductive probe signal decay as a function of distance from the accelerator. Helium at a pressure of 5μ Hg	34

FIGURE	PAGE
17. Air. (Upper) electron-ion difference current in microamps as a function of magnetic field, (lower) relative light outputs corresponding to currents above.	35
18. Helium. (Upper) electron-ion difference current in microamps as a function of the magnetic field, (lower) outputs corresponding to currents above	36
19. Schematic of experimental setup to make simultaneous light output and current output measurements	37

I. INTRODUCTION

The interaction of microwaves with ionized gases has recently become an area of intense investigation, and microwave circuit components utilizing concepts learned from these investigations are already in production. Weibel (1)* has suggested using microwaves to confine a plasma column. Brown (2,3) has made an extensive study of high frequency gas-discharge breakdown and has compiled a large amount of data.

Radiation pressure had been considered primarily as a means of confining plasmas until Hess and Thom (4) of the National Aeronautics and Space Administration, Langley Research Center suggested using microwave radiation pressure for accelerating plasmas. Additional impetus has been given to the latter suggestion by the recent development of high power microwave sources (of the order of 10^8 watts peak power).

The radiation pressure method of acceleration has a distinct advantage over the electrical propulsion systems in that the problems of coupling the electromagnetic energy to the plasma are greatly reduced. The energy from guided microwaves is already unidirectional, therefore eliminating the need for schemes to convert the microwave energy to kinetic energy of the plasma. This advantage exists, of course, only for highly absorptive or reflective plasmas. Plasmas that are transparent to electromagnetic waves would not experience any force.

The problem in general, is to investigate various schemes of "pushing" plasmas with electromagnetic waves, and to develop diagnostic

*Numbers in () refer to references stated in the bibliography.

techniques to measure these effects; in particular, it was decided to attempt to produce and accelerate a plasma by means of microwaves from a radar transmitter. Using such a transmitter, a plasma was produced in a partially evacuated section of coaxial transmission line by radio frequency breakdown and the plasma was then accelerated into a glass tube by radiation pressure and diffusion. An axial magnetic field was used for channeling to prevent the plasma from diffusing to the walls of the glass tube before having traveled the length of the tube. The plasma was detected and its velocity measured downstream with photo-cells and induction probes. Velocities as high as $2.4 \times 10^6 \frac{\text{m}}{\text{sec}}$ ± 15 percent were obtained. The experiments were conducted using both helium and air and the results are compared.

II. ACCELERATION OF A PLASMA BY RADIATION PRESSURE

Definition of a plasma.- A plasma, for the purposes of this paper, may be considered as a fully or partially ionized gas which is nearly space charge neutral; that is, the number of electrons in a unit volume equals the number of singly charged positive ions in that volume, assuming negative ions are not present. A plasma, then, can be said to consist of three distinct component "gases," namely, the electron gas, the ion gas, and a gas consisting of the neutral molecules.

In a plasma, there is always a recombination of positive ions and electrons to form neutral molecules. At the same time, there is also ionization of neutral molecules due to collisions with other particles. Under certain conditions, such as those present in the earth's ionosphere and stellar atmospheres, the rate of production of ions and electrons equals the rate of recombination of electrons with ions, and a steady-state situation exists in the relative numbers of electrons, ions, and neutral molecules. If the rate of production is greater than the recombination rate, then the gas will eventually become fully ionized. However, if the rate of production is less than the rate of recombination, then there will be a net loss of charged particles and the plasma is said to be in decay.

Force exerted on a reflecting surface by electromagnetic radiation.

Since a plasma is a conductor of electricity, it can reflect incident electromagnetic radiation, and since such radiation is the carrier of momentum, the reflection will result in a force on the plasma. An expression for this force can easily be found as follows.

The momentum carried by a photon of energy $h\nu$ is $\frac{h\nu}{c}$ and thus unidirectional electromagnetic radiation which transports energy E will carry momentum $\frac{E}{c}$, where c is the velocity of the radiation. But $dE/dt = P$ where P is the power and t the time. The rate of transport of momentum, from above is thus:

$$\frac{1}{c} \frac{dE}{dt} = \frac{P}{c}$$

Now if a fraction f of the radiation incident on the plasma is reflected, the rate of change of momentum of the plasma will be

$$(1 + f) \frac{P}{c}$$

and this is, by Newton's second law, the force exerted by the radiation.

For total reflection

$$f = 1$$

and

$$F = \frac{2P}{c}$$

III. PRODUCTION AND MEASUREMENT OF THE PLASMA

Radio frequency breakdown.- In a high frequency gas discharge breakdown, the primary ionization from the electron motion is the only production phenomenon that controls the breakdown. If one calculates the maximum kinetic energy in the oscillatory motion of an electron at the minimum field intensities for which breakdown is observed experimentally, one finds a value of about 10^{-3} electron volt. This is obviously insufficient to supply the ionization potential of several volts required for breakdown.

It is well known that a free electron in a vacuum under the action of an alternating electric field oscillates with its velocity 90° out of phase with the field, and thus takes no power, on the average, from the applied field. The electron can gain energy from the field only by suffering collisions with the gas atoms, and it does so by having its ordered oscillatory motion changed to random motion on collision. The electron gains random energy, on the average, on each collision until it is able to make an inelastic collision with a gas atom.

When an external d-c magnetic field is applied in the situation described above, the electrons have another means by which they can gain energy from the electric field. In the case of high frequency breakdown in a magnetic field, considering collisions, the medium becomes anisotropic and the effective dielectric constant becomes a tensor given, as shown in appendix A by

$$\epsilon = \begin{vmatrix} \epsilon_{11} & i\epsilon_{12} & 0 \\ -i\epsilon_{12} & \epsilon_{11} & 0 \\ 0 & 0 & \epsilon_{33} \end{vmatrix}$$

where

$$\epsilon_{11} = 1 - \omega_p^2 \left\{ \frac{(\omega^2 - \omega_c^2 + \nu^2) - i\left(\frac{\nu}{\omega}\right)(\omega^2 + \omega_c^2 + \nu^2)}{[(\omega + \omega_c)^2 + \nu^2][(\omega - \omega_c)^2 + \nu^2]} \right\}$$

$$\epsilon_{12} = \omega_p^2 \omega_c \left\{ \frac{\left(\frac{1}{\omega}\right)(\omega_c^2 - \omega^2 + \nu^2) + 2i\nu}{[(\omega + \omega_c)^2 + \nu^2][(\omega - \omega_c)^2 + \nu^2]} \right\}$$

$$\epsilon_{33} = 1 - \omega_p^2 \left\{ \frac{1 - i\left(\frac{\nu}{\omega}\right)}{\omega^2 + \nu^2} \right\}$$

and

ω microwave frequency, radians/sec

ω_p plasma frequency

ω_c electron cyclotron frequency

ν electron-neutral molecule collision frequency, (C/sec)

ϵ_0 free space dielectric constant

Since the imaginary part of the dielectric constant represents the losses to the medium, the maximum energy transfer from the microwave field to the electrons occurs when the imaginary part of the dielectric constant is a maximum. This occurs at

$$\omega = \omega_c$$

This causes a resonance effect and is called "electron cyclotron resonance."

For these experiments, the resonance effect occurred at about 1020 gauss as will be seen in figures 17 and 18.

Velocity measurements.- The majority of the velocity measurements were made using a photocell as a detector.

The pulse produced by the luminous front passing the photocell was displayed on an oscilloscope triggered at a fixed time with respect to the microwave pulse initiating the plasma. Observations were repeated as the photocell was moved farther downstream from the accelerator; the pulse was displaced in time on each succeeding oscillogram. The displacement corresponds to the time required for the front to move the distance the photocell has been moved. The velocity of the luminous front can easily be calculated from the displacements.

Other velocity measurements were made by means of an induction probe. When the plasma travels down the glass tube, it passes through a cylindrical brass probe surrounding the tube; the charged particles induce a voltage in the probe and the signal is displayed on an oscilloscope. The signals from the electrons and the ions do not cancel each other because they do not arrive at the probe at the same time. The velocity of the plasma is determined from these induction probe signals in a manner analogous to that used for the photocell method.

IV. APPARATUS

Description of equipment used for producing the plasma.- The plasma is produced by radio frequency breakdown in an evacuated coaxial chamber, henceforth called the accelerator and shown schematically in Figure 1. A complete list of all equipment with manufacturer's names and model numbers appears in appendix B. The source of the radio frequency energy is an SCR-984 radar transmitter utilizing a 2J31 magnetron. The peak power output of the magnetron is 250 kw at a frequency of 2.85 kmc. In order to increase the available energy per pulse the normal transmitter pulse length has been increased from 0.8 microsecond to 1.0 microsecond.

The energy is fed to the accelerator through an S-band waveguide circuit shown in Figure 1. The isolator provides a 20-db attenuation for signals reflected from the breakdown or from the mismatch at the end of the coaxial cable in the accelerator, preventing the magnetron from being influenced by these signals. An E-H plane tuner is used for matching the waveguide circuit for maximum power transmission from the magnetron to the accelerator. The remainder of the microwave components shown in Figure 1 were not used in this investigation.

Two sets of Helmholtz coils, wound on aluminum spools and shown in Figure 2, were used to produce a magnetic field in the breakdown region. The four coils are mounted on the same axis. In order to preserve the Helmholtz coil geometry the outer two coils had to be larger than the inner two. The outer coils were 23 inches in diameter and the inner coils were 21 inches in diameter. Uniform magnetic fields of up to 1500 gauss with less than 5 percent variation can be produced over a

region about 20 cm long and 10 cm in diameter. In order to retain constant field strengths for periods of up to 30 seconds, it was necessary to introduce cooling devices. One and one-eighth OD copper tubing was rolled into a rectangular cross section of about 1/4 inch by 1-3/4 inches. After each 10 turns of wire on the coils, one of these copper cooling strips, blanked off at each end with an inlet or outlet tube, was wrapped around the turns. On the larger coils, two cooling strips were needed and on the smaller ones only one was necessary.

The resistance of the four coils combined was 3 ohms and currents up to 150 amps were passed through them. The power supply was a d-c generator having a maximum output capability of 750 amps at 600 volts.

Accelerator.- The entire accelerator is machined from brass and is shown in a sectional drawing in Figure 4. The particular gas being used is fed in through the gas inlet tube. The pressure at the breakdown point is monitored with an ionization gage, and in the glass tube with a Hastings thermocouple gage.

The coaxial cable from the S-band waveguide circuit leads directly into the accelerator. As can be seen in Figure 4, the continuity of the coaxial line has been preserved right through the accelerator. The Teflon "window" provides the vacuum seal in the coaxial cable. Two of the Teflon "windows" that were used in these experiments are shown along with the brass center conductor in Figure 5.

Plasma detection equipment:- The diagnostic work in these experiments was concerned mainly with detecting the plasma as it passed some position along the glass tube. Two methods of detection were used. The first employed a photocell, the second an induction probe.

The photocell method is shown schematically in Figure 1. The coil wrapped tightly around the glass tube produces an axial magnetic field in the tube and prevents the plasma from diffusing to the walls. The "gaps" in the coil are evenly spaced 10 cm apart and are each 1 cm wide. These "gaps" are the stations at which the photocell "sees" the plasma. It was necessary to paint the entire inside of the glass tube with flat black paint, except for small openings at the "gaps" in the coil around the tube in order to eliminate internal reflections of light from the luminous front which would be detected by the photocells long before the front arrival at the photocell, thus giving erroneous results.

In order that all the oscillograms have a common origin for a reference point, it was necessary to trigger the oscilloscope at the same time with respect to the discharge for each oscillogram. This was done by synchronizing the oscilloscope with the microwave pulse producing the breakdown. The pulse generator used to trigger the driver unit in the SCR-584 has a second output allowing simultaneous triggering of two events. The pulse from the second output was passed through a variable time delay generator, and then to the external trigger input on the oscilloscope. Every time a pulse was sent to the driver unit to drive the magnetron, another pulse was sent to the external triggering circuit on the oscilloscope. The time delay generator was adjusted until the signal from the photocell appeared on the oscilloscope screen in a convenient position and was then left at that setting for the remaining measurements.

Typical velocity measurement signals from the photocells are shown in the oscillograms of Figures 7 and 8.

For the induction probe measurements, the glass tube used for the photocell measurements was replaced with a glass tube without a coil around it. An induction probe, which was simply a ring 1.0 cm wide and 7.6 cm in diameter fabricated from 1/16-inch brass sheet stock, was designed to slide over the outside of the glass tube. When either positive or negative charges pass through such a ring they induce a voltage in the ring. Velocity measurements are made using these signals in exactly the same manner as that described in connection with photocell measurements. Oscillograms of these signals are shown in Figures 9 and 10.

Signal decay measurements.- In order to determine whether the luminous front represented a moving plasma or a stream of electrons exciting gas atoms as they proceeded down the tube, light output measurements were made as a function of distance from the accelerator and compared with similar signals from the induction probe. The sensitivity and the sweep rate of the oscilloscope were decreased so that the entire signal from the photocell was displayed. Oscillograms were made of this signal at each station along the glass tube, and the maximum amplitudes are shown as functions of distance from the accelerator in Figures 11 and 12. The oscillograms of the photocell signals appear in Figures 13 and 14.

Oscillograms were also made of the signals from the induction probe at every 10 cm along the tube. The maximum amplitudes of those parts of the signals produced by the electrons were also shown in Figures 11 and 12.

FROM BERTIN & BERTIN TO SECTION

The signals produced by the ions decay to zero a short distance from the accelerator. The oscillograms of the induction probe signals are shown in Figures 15 and 16.

Total current output measurements.- Another probe, used to measure the difference in electron and ion emission currents from the accelerator was also made from 1/16-inch brass sheet stock. This probe was a cylinder 7.0 cm in diameter and 100 cm long. This probe was fitted inside the glass tube and collected all charges emitted from the accelerator. As can be seen in Figure 19, the probe is connected directly to an ammeter the other side of which was connected to the accelerator which was at ground potential. Since the microwaves were pulsed, the currents from the accelerator were pulsed, an 8 μ f capacitance was connected in parallel with the ammeter in order to measure average currents.

Currents were measured as a function of the external magnetic field produced by the Helmholtz coils and the data may be found in Figures 17 and 18. At the same time, the total light output was monitored by a photocell "looking" into the accelerator from the end of the tube; the amplitudes of the signals from this photocell are also shown in Figures 17 and 18.

Vacuum system.- The vacuum system was designed to quickly evacuate the accelerator and glass tube to a pressure of 0.01 μ Hg. The operating range of the diffusion pump is 3×10^{-4} to 2×10^2 μ Hg with a maximum pumping speed of 210 liters per second at 8 μ Hg. As shown in the schematic drawing of the vacuum system in Figure 6, the diffusion pump could be completely shut off from the rest of the system to prevent contamination and cooling of the diffusion pump oil every time that air

was admitted to the system. The system was opened several times to the atmosphere during a day's operation to insert different probes. Operation was mostly in the 1 to 10 μ Hg range and occasionally, higher pressures were used.

V. INTERPRETATION OF DATA

Analysis of velocity measurements.- The results of some of the velocity measurements described in chapter IV are tabulated in Table I. The average velocity in air, using both photocell and induction probe measurements was $2.2 \times 10^6 \frac{\text{m}}{\text{sec}}$ ± 11 percent. The average velocity in helium was $2.4 \times 10^6 \frac{\text{m}}{\text{sec}}$ ± 13 percent.

When it was possible to maintain the breakdown, velocity measurements were made without the external magnetic field, and the velocities were found to be in the same range as those obtained with the external field. The velocities measured were independent of the magnetic field in the breakdown region. According to the theory of the effect of a d-c magnetic field on high frequency breakdown (5), the electrons emitted from the accelerator when an external magnetic field is applied should be more energetic than those emitted without an external magnetic field. The fact that the velocities of the luminous front and the electrons were independent of the magnetic field gave rise to further experiments to determine the nature of the luminous front and the origin of the electrons; simultaneous measurements were made of light output and induction probe signals as a function of distance from the accelerator. Also, simultaneous measurements were made of total light output and current output from the accelerator.

Comparison of signal decay measurements.- The signal decay measurements described in chapter IV were made to help determine whether the luminous front was caused by a moving plasma or a stream of electrons exciting gas molecules as they moved down the tube. The maximum amplitudes of the light and of the induction probe electron current signals are

TABLE I.- VELOCITY MEASUREMENT DATA

Run no.	PHOTOCELLS		INDUCTIVE PROBE	
	AIR	HELIUM	AIR	HELIUM
1	$2.2 \times 10^6 \frac{m}{sec}$	$2.8 \times 10^6 \frac{m}{sec}$	$2.3 \times 10^6 \frac{m}{sec}$	$2.6 \times 10^6 \frac{m}{sec}$
2	2.4	1.7	1.9	2.3
3	1.2	3.2	2.2	2.1
4	3.0	1.9	2.1	2.4
5	2.0	2.2	1.8	2.5
6	2.6	2.2	2.4	1.9
7	1.9	2.4	2.7	2.1
8	2.3	2.3	2.1	2.3
9	2.2	2.8	2.3	2.2
10	2.3	3.1	2.2	2.4
Mean:	2.2×10^6	2.4×10^6	2.2×10^6	2.3×10^6
Standard deviation	0.3	0.4	0.2	0.2

plotted against distance from the accelerator in Figures 11 and 12. The decay of the two signals in air as shown in Figure 11 would indicate that the electron stream and the luminosity are definitely related. However, the measurements in helium, plotted in Figure 12 do not readily show such a relationship. A possible explanation of the shape of the inductive probe signal decay curve in Figure 12 is that the mobility of helium ions in a helium atmosphere is much greater than the mobility of molecular air ions in an air atmosphere. Therefore, the helium ions travel farther and faster than the ions from the air breakdown and decrease the effective negative signal induced in the probe. The increase in the negative signal between the 20-cm and 70-cm points is then due to the loss of positive ions to the walls of the glass tube. It is possible that in the experiments performed with helium, a plasma moves as far as 60 cm from the accelerator.

Effect of magnetic field on breakdown.- In the upper half of Figures 17 and 18, the difference between the total electron and ion currents emitted from the accelerator is plotted against the magnetic field. These curves show that the electron current exceeds the positive ion current except for that part of the curve for helium above 915 gauss. For the latter, the ion current exceeds the electron current. The lower parts of Figures 17 and 18 are total light output measurements made simultaneously with the current readings above.

In air the light output remains constant until electron cyclotron resonance occurs. In helium, the light output follows the electron outputs and above 915 gauss it follows the ion current output.

As stated above, measurements made at different magnetic field strengths did not indicate that more energetic particles come from the accelerator at higher magnetic fields.

Considering the long electron mean free path at these pressures (26.5 cm in He at 5μ and 8.9 cm in air at 5μ Hg) compared to the breakdown region dimensions in the direction of the electric field, it is very unlikely that the breakdown is diffusion controlled. The ratios of electron mean free paths to the radial dimensions of the breakdown region at a pressure of 5μ Hg for helium and air are 48 and 16, respectively. The probability of an electron having an ionizing collision with a gas molecule is therefore small. The breakdown is more likely controlled by secondary electrons from the walls of the accelerator due to electron bombardment. This could account for the apparent independence of the particle velocities on the magnetic field. That is, the electrons receive more energy from the microwave field as a result of the external magnetic field, but this energy is used mostly in releasing more particles from the accelerator walls. Some of the energy is also expended in heating the accelerator walls.

Electromagnetic force on the plasma.- We shall estimate the electromagnetic force on the plasma, using the same expression which holds in free space. This is a good approximation since in a coaxial cable the principal mode of transmission is the TEM mode - that is, the energy is almost all in the transverse fields. Under our conditions, the microwaves may be assumed totally reflected since the skin depth "d" in the plasma is small compared to the length of the breakdown region. The skin depth is given by the expression (6)

$$d = \frac{c}{\omega_p} \left[\frac{1}{1 - \frac{\omega^2}{\omega_p^2}} \right]^{1/2}$$

where ω_p is the plasma frequency and is

$$\omega_p = \left[\frac{4\pi n_e e^2}{m_e} \right]^{1/2}$$

where

- n_e electron density
- e charge on the electron
- m_e electron mass

Assuming a 1-percent ionization (which is probably high for this type of breakdown), the plasma frequency is

$$\omega_p = 5.64 \times 10^{10} \frac{\text{cycles}}{\text{sec}}$$

and the skin depth for $2.85 \times 10^9 \frac{\text{cycles}}{\text{sec}}$ microwaves is

$$d = 0.532 \text{ cm}$$

In these experiments, the coaxial breakdown chamber was approximately 15 cm long, or nearly 30 times the skin depth.

As was shown above, the relationship between the force exerted by the microwaves and the power is

$$F = \frac{2P}{c}$$

for a reflecting surface. The microwave peak power used in these experiments was 250 kw. The force on a perfectly reflecting plasma

would thus be:

$$F = \frac{2 \times 2.50 \times 10^3}{3 \times 10^8} = 1.67 \times 10^{-2} \text{ newtons}$$

Assuming the breakdown to occur over a 0.02-m length in the accelerator, a volume of $5.3 \times 10^{-6} \text{ m}^3$ would become partially ionized. At a pressure of $5\mu \text{ Hg}$ the particle density is approximately 10^{20} particles m^3 . For air this would represent a mass of about $2.5 \times 10^{-15} \text{ kg}$. The force from the microwaves acts for $1\mu \text{ sec}$. Assuming the entire mass of the gas is accelerated, the velocity would be

$$v = \frac{Ft}{m} = \frac{1.76 \times 10^{-2} \times 10^{-6}}{2.5 \times 10^{-15}} = 6.6 \times 10^6 \frac{\text{m}}{\text{sec}}$$

This velocity is approximately three times larger than the measured velocities.

Use of the total mass of the gas in the breakdown region, which is equivalent to assuming good contact between the ions and neutrals, gives a lower limit for the velocity attainable from this microwave power; if, as is likely, only the charged particles were accelerated, a much higher velocity would result.

The total mass accelerated was not measured and therefore the efficiency of energy conversion cannot be calculated.

VI. CONCLUSION

A low density plasma was produced by microwave breakdown in an evacuated coaxial chamber. It was shown that in the case of helium a moving plasma was detected as far as 60 cm from the accelerator at a velocity of $2.4 \times 10^6 \frac{\text{m}}{\text{sec}} \pm 15$ percent. It was also shown that the external magnetic field did not affect the velocity of the plasma, but did influence the output current from the accelerator.

Other microwave plasma accelerator designs are now under consideration by the author. To produce larger accelerating forces on the plasma, continuous wave microwave systems may be used. Also the plasma might be injected into the system rather than be produced and accelerated by the same energy source.

GENERATION AND ACCELERATION OF PLASMA

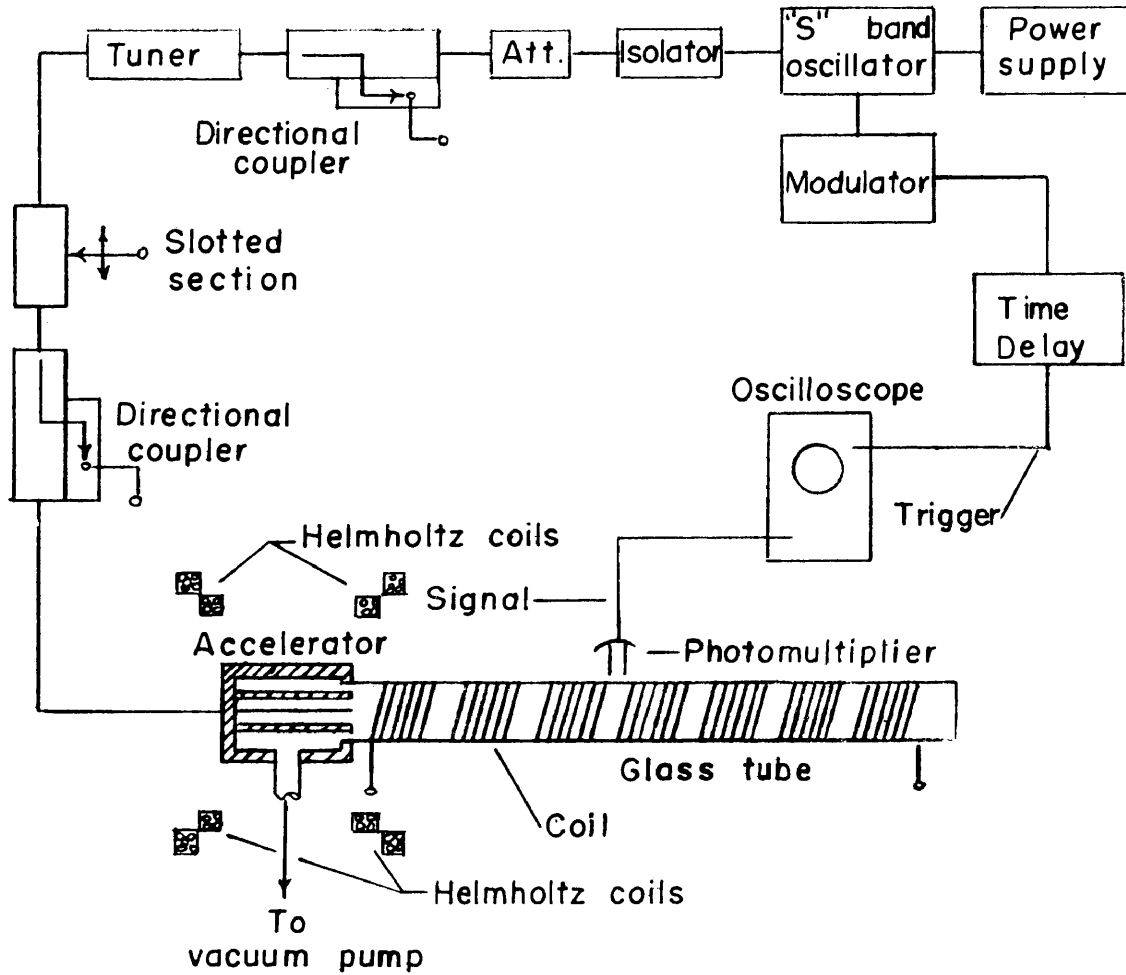
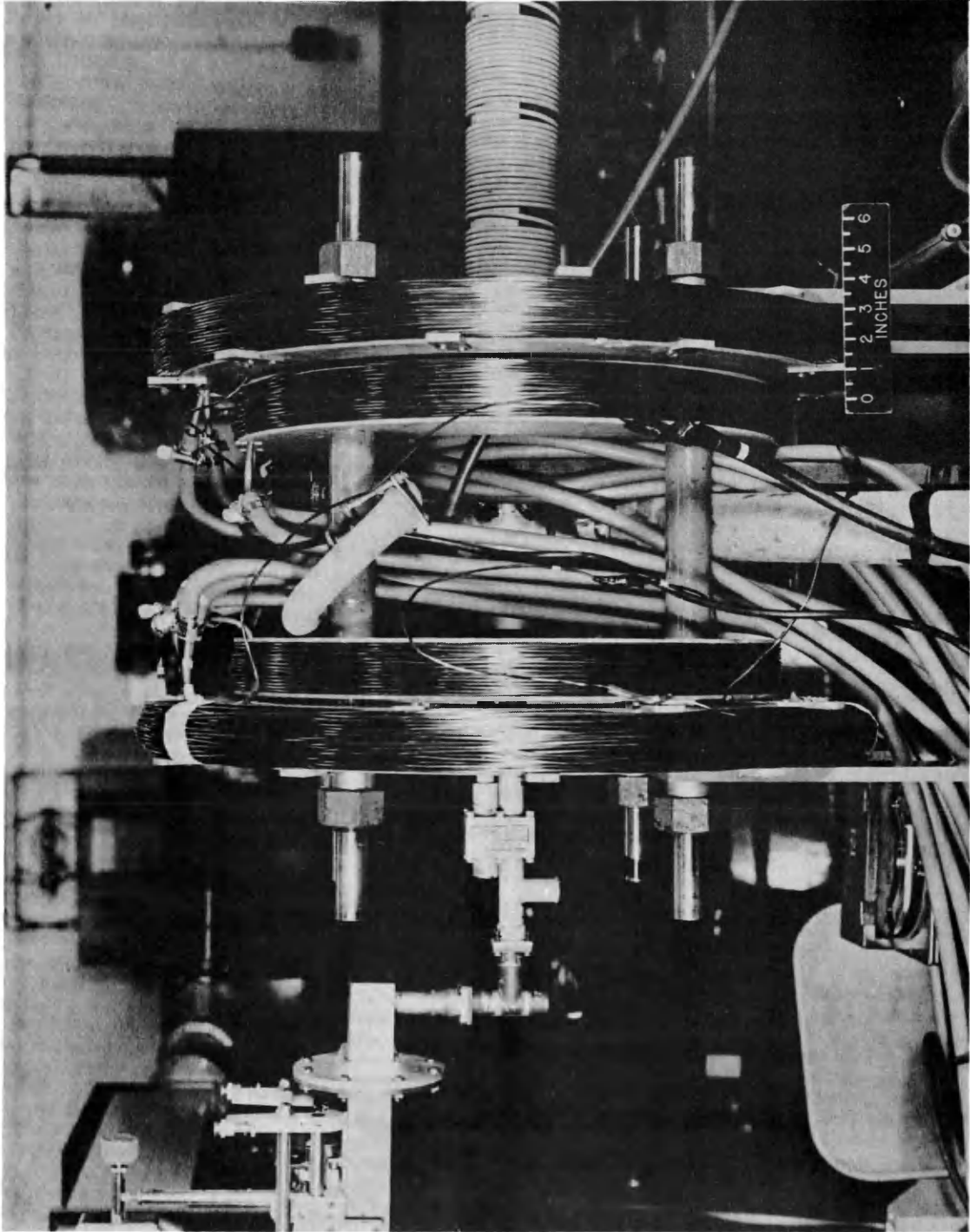


Figure 1.- Schematic of microwave circuit and method of making velocity measurements using photocells.



L-60-7805

Figure 2.- Helmholtz coils.

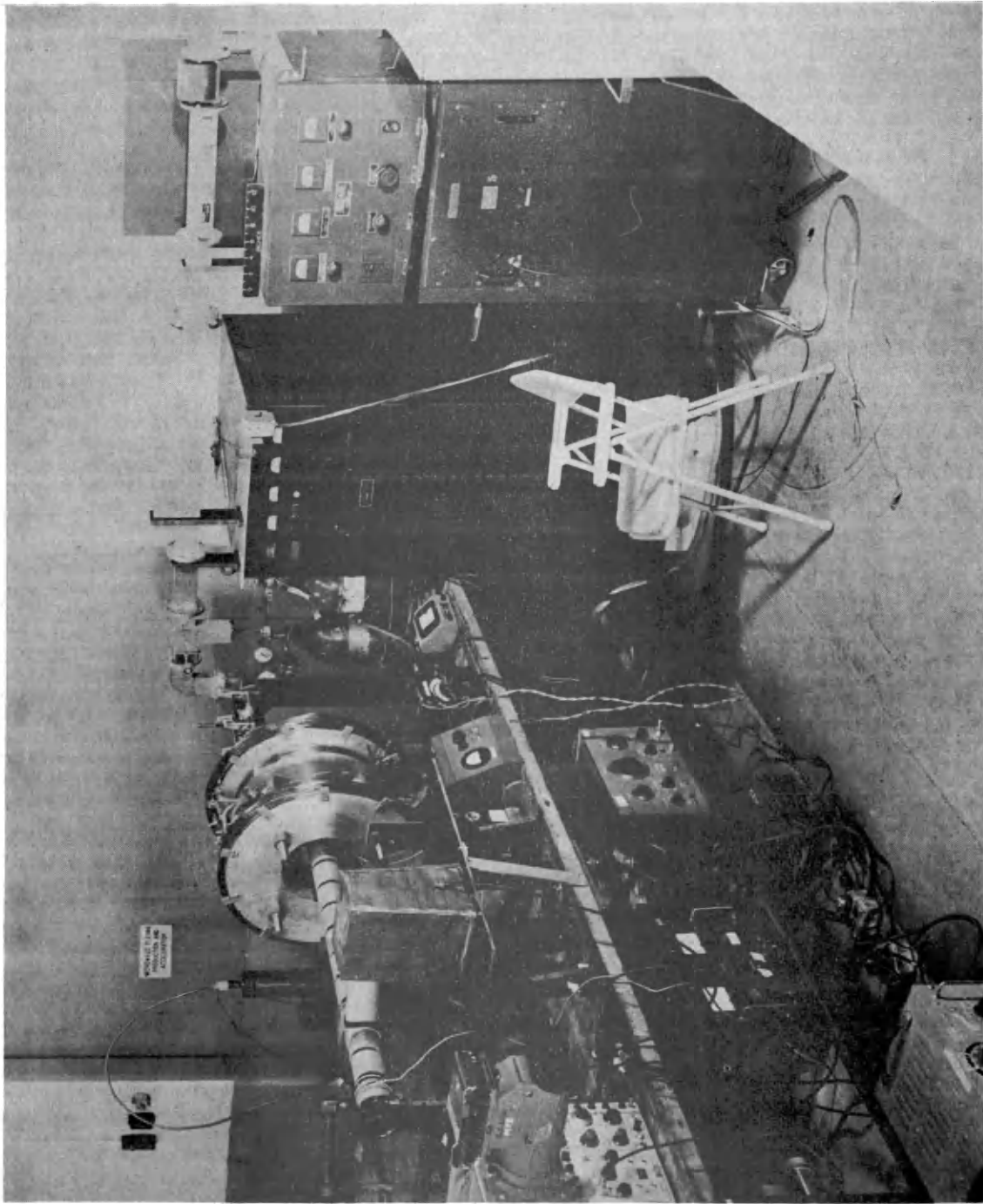


Figure 3.- Entire experimental setup. L-60-7806

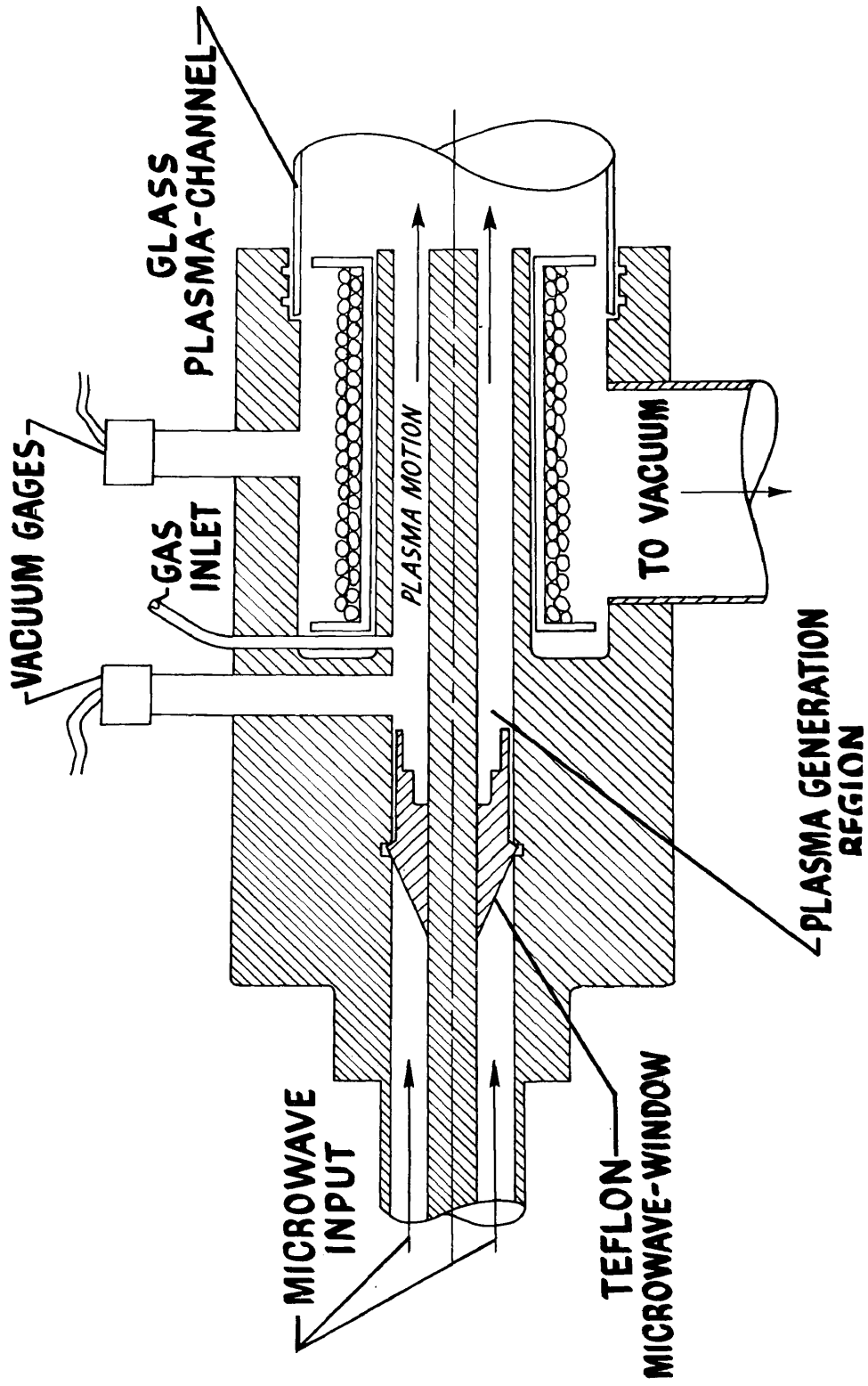


Figure 4.- Coaxial accelerator. I-60-7807

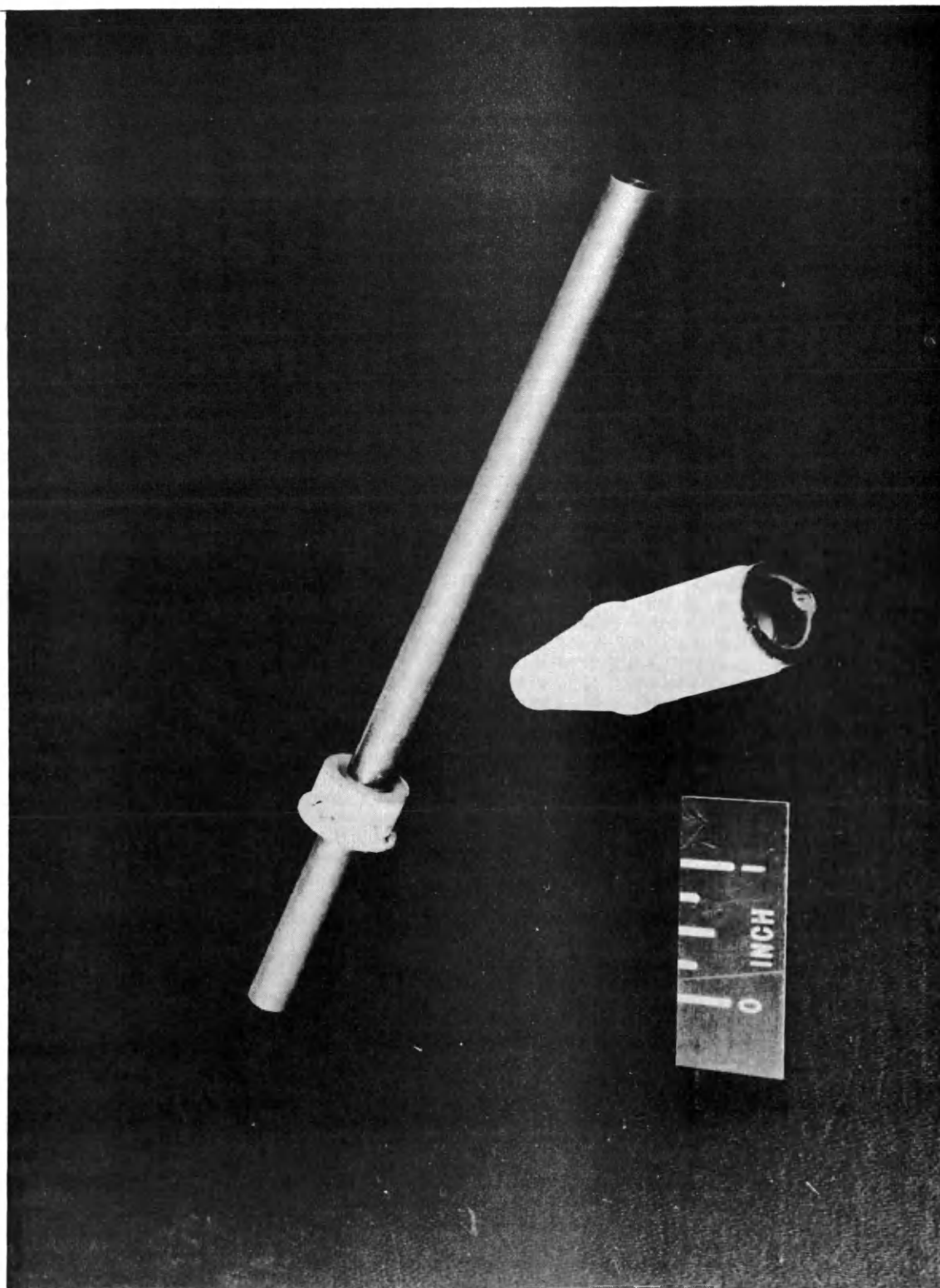


Figure 5.- Two Teflon "windows" and center conductor. L-60-7804

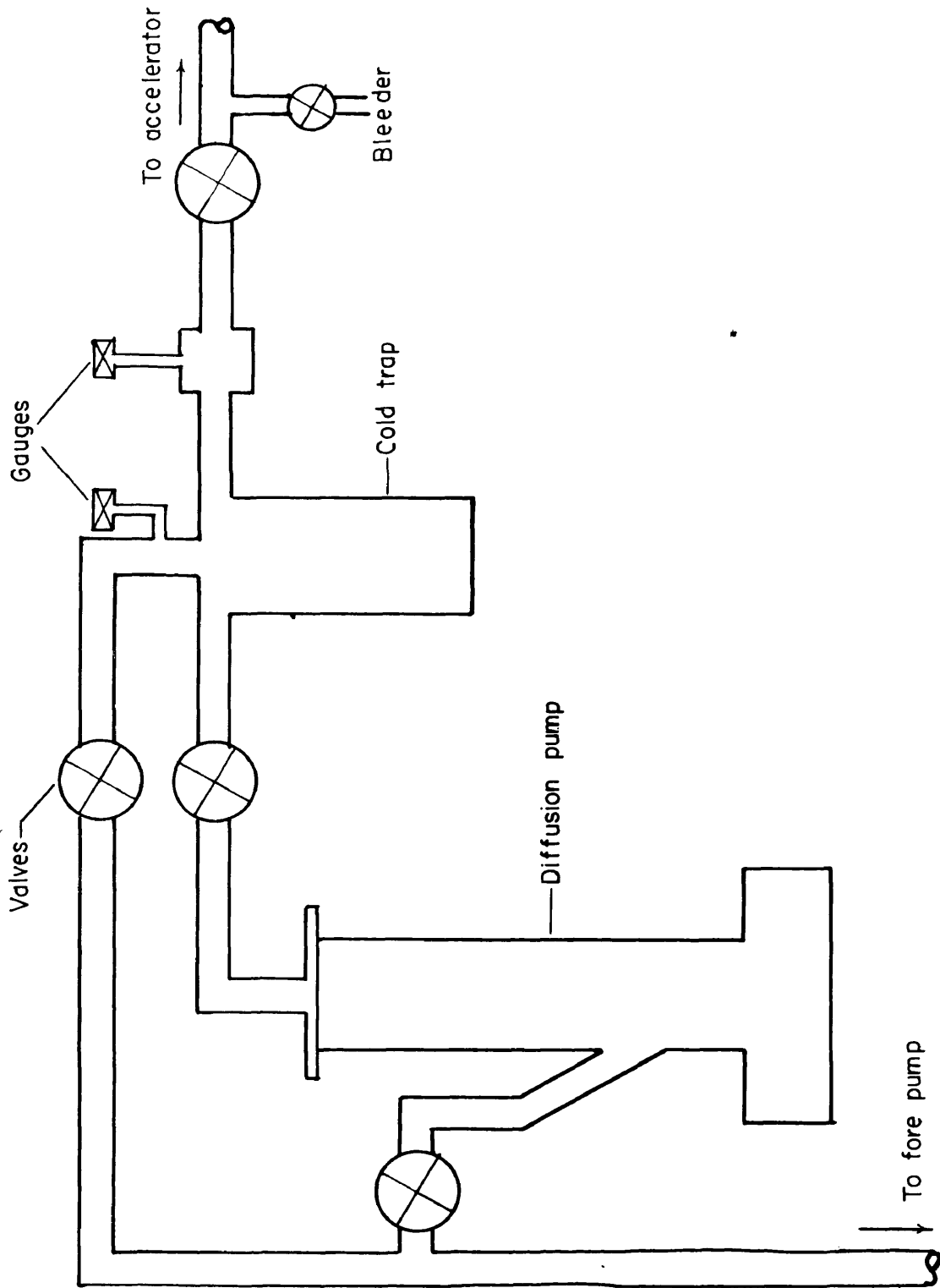


Figure 6.- Vacuum system.

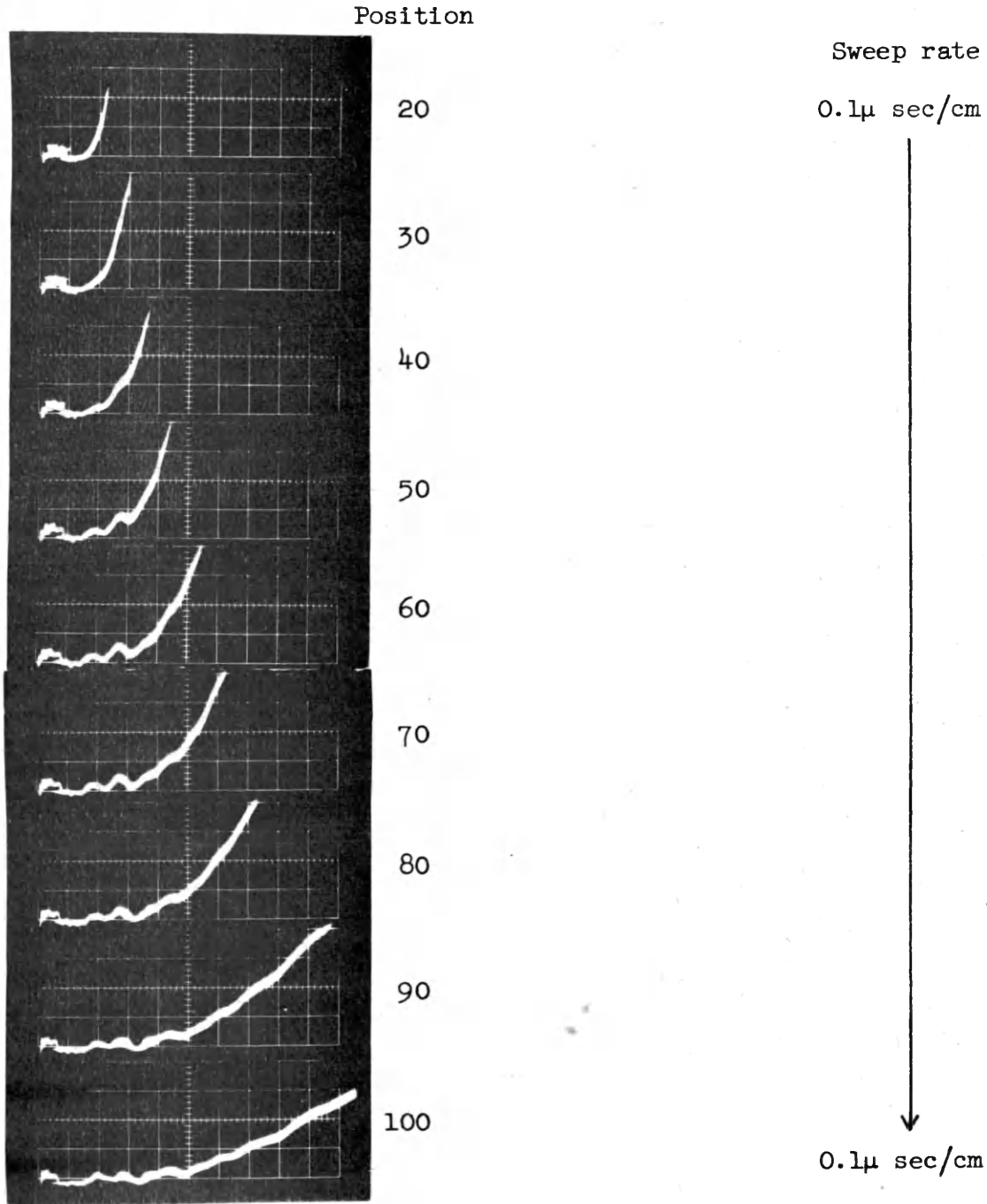


Figure 7.- Velocity runs with photocells. Air at a pressure of 5μ Hg.

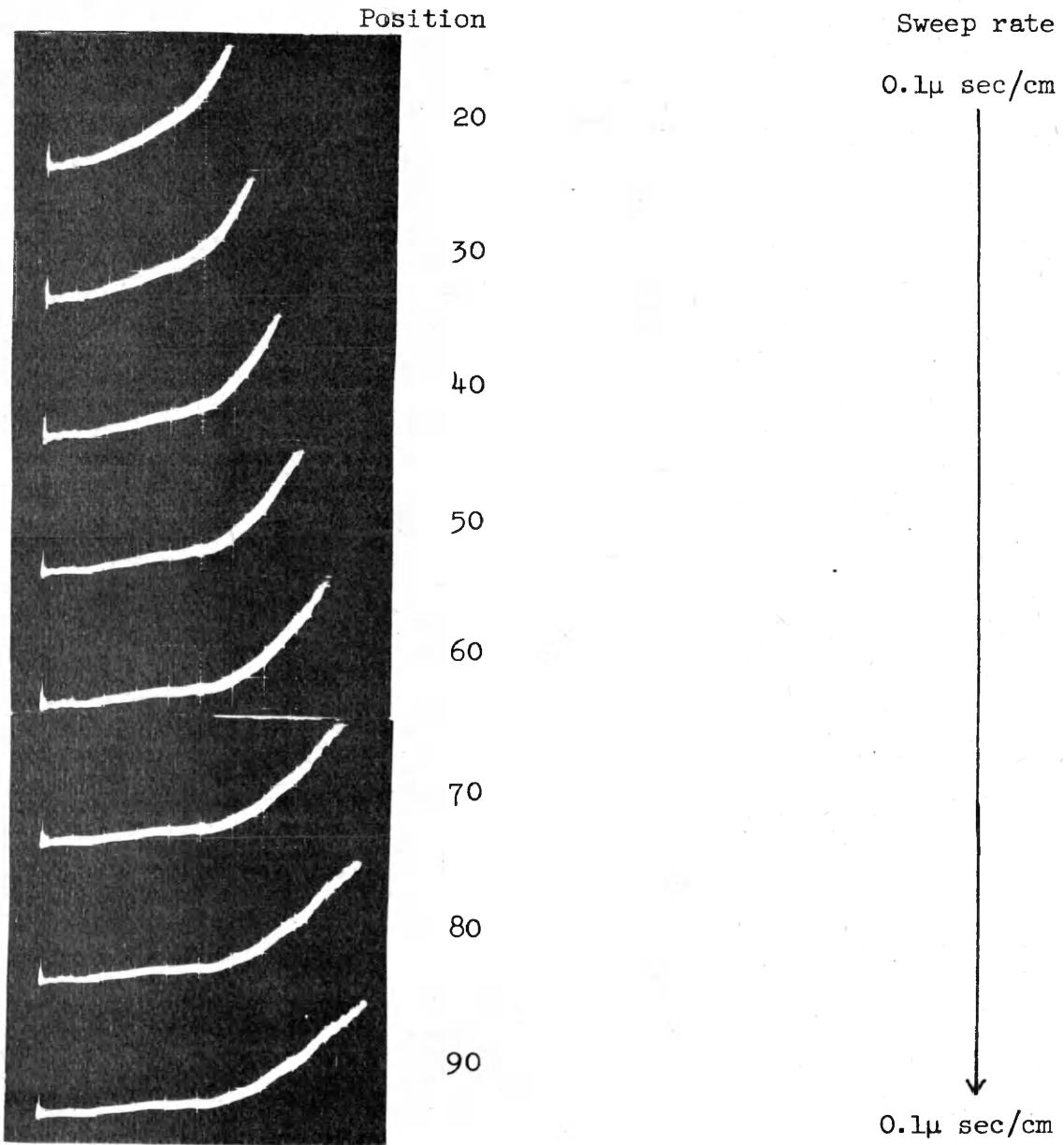


Figure 8.- Velocity runs with photocells. Helium at a pressure of 5 μ Hg.

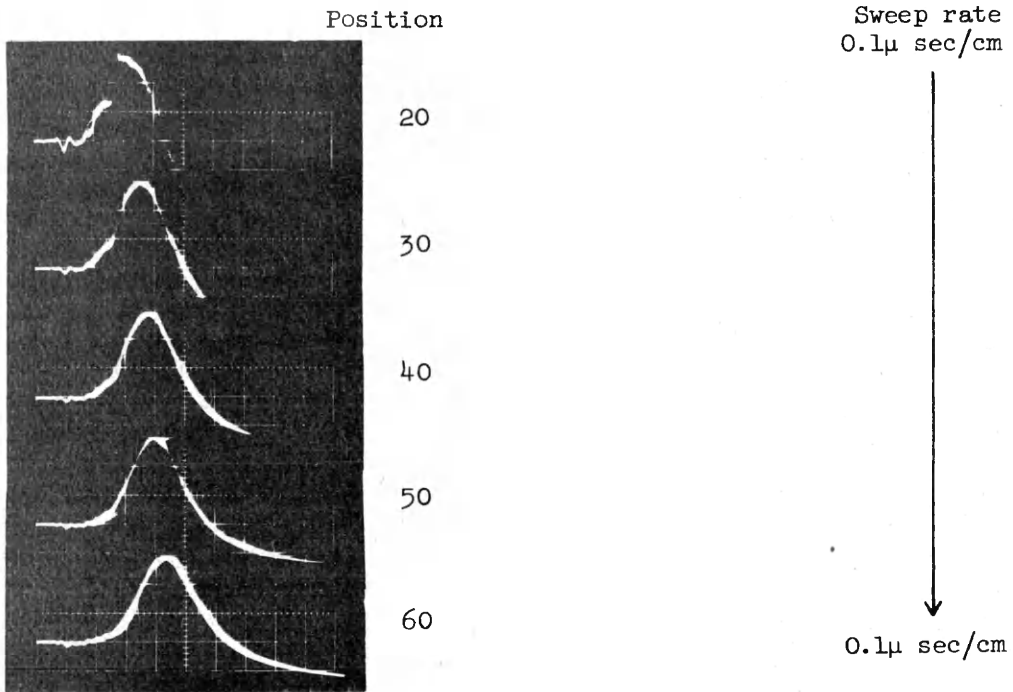


Figure 9.- Velocity runs with induction probe, air.

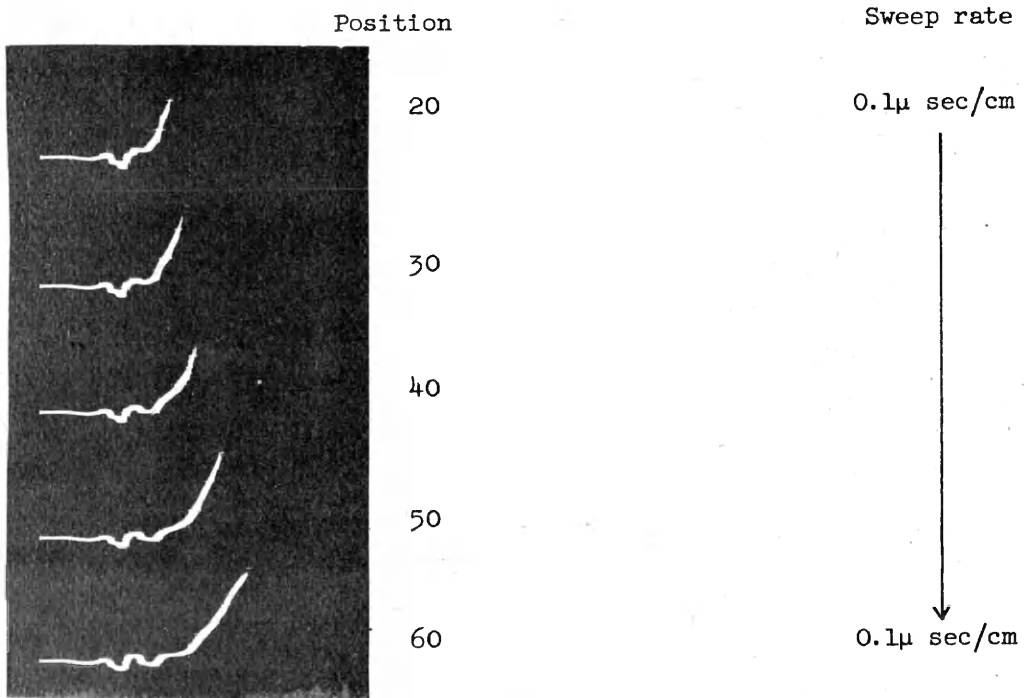


Figure 10.- Velocity runs with induction probe, helium.

AMPLITUDE (NORMALIZED) VS DISTANCE

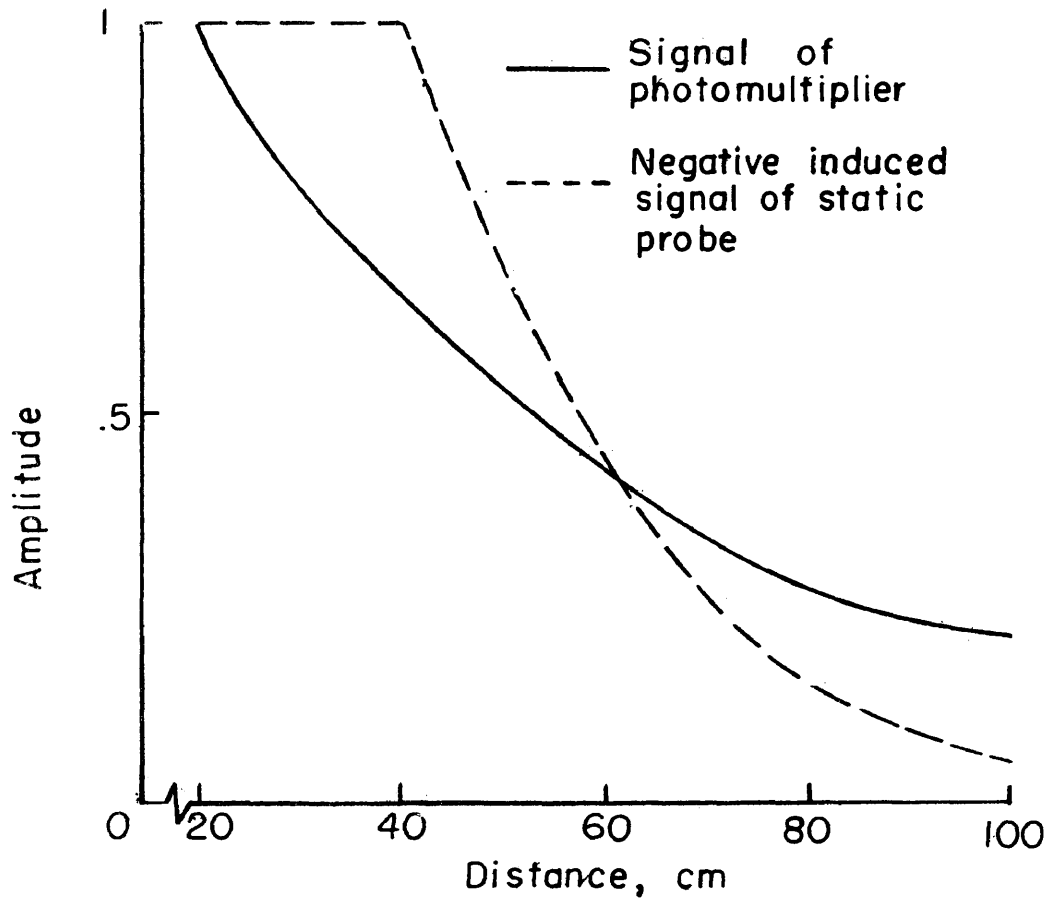


Figure 11.- Comparison of light signal decay to induction probe signal decay as a function of distance from the accelerator, air.

AMPLITUDE (NORMALIZED) VS DISTANCE

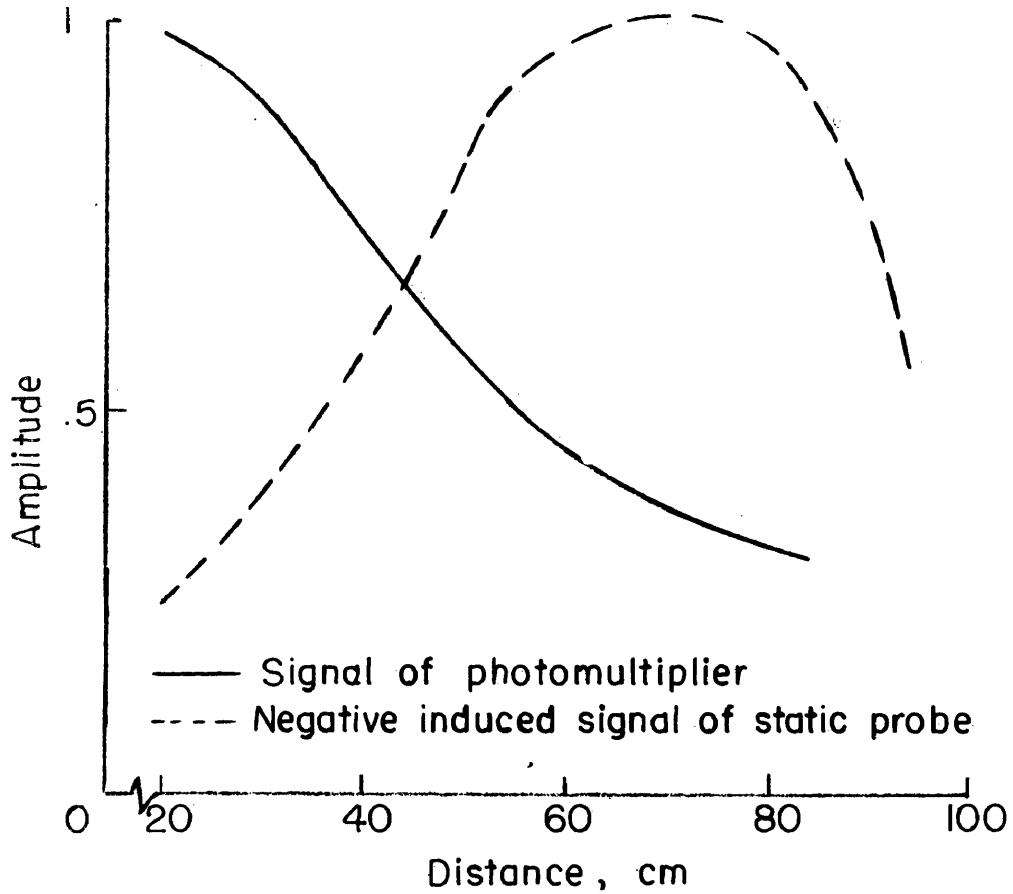


Figure 12.- Comparison of light signal decay to inductive probe signal decay as a function of distance from the accelerator, helium.

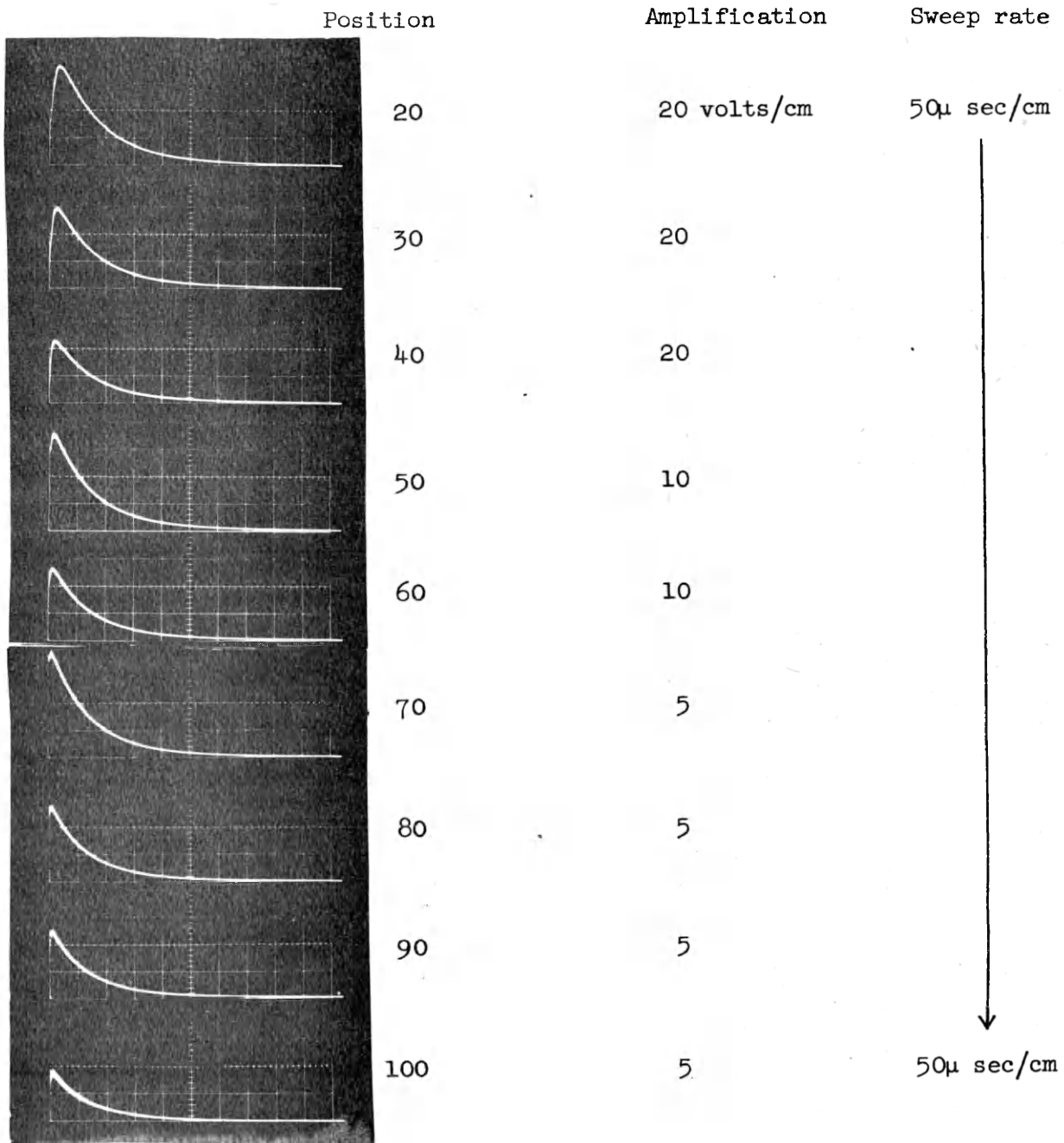


Figure 13.- Light decay as a function of distance from accelerator. Air at a pressure of 5 μ Hg.

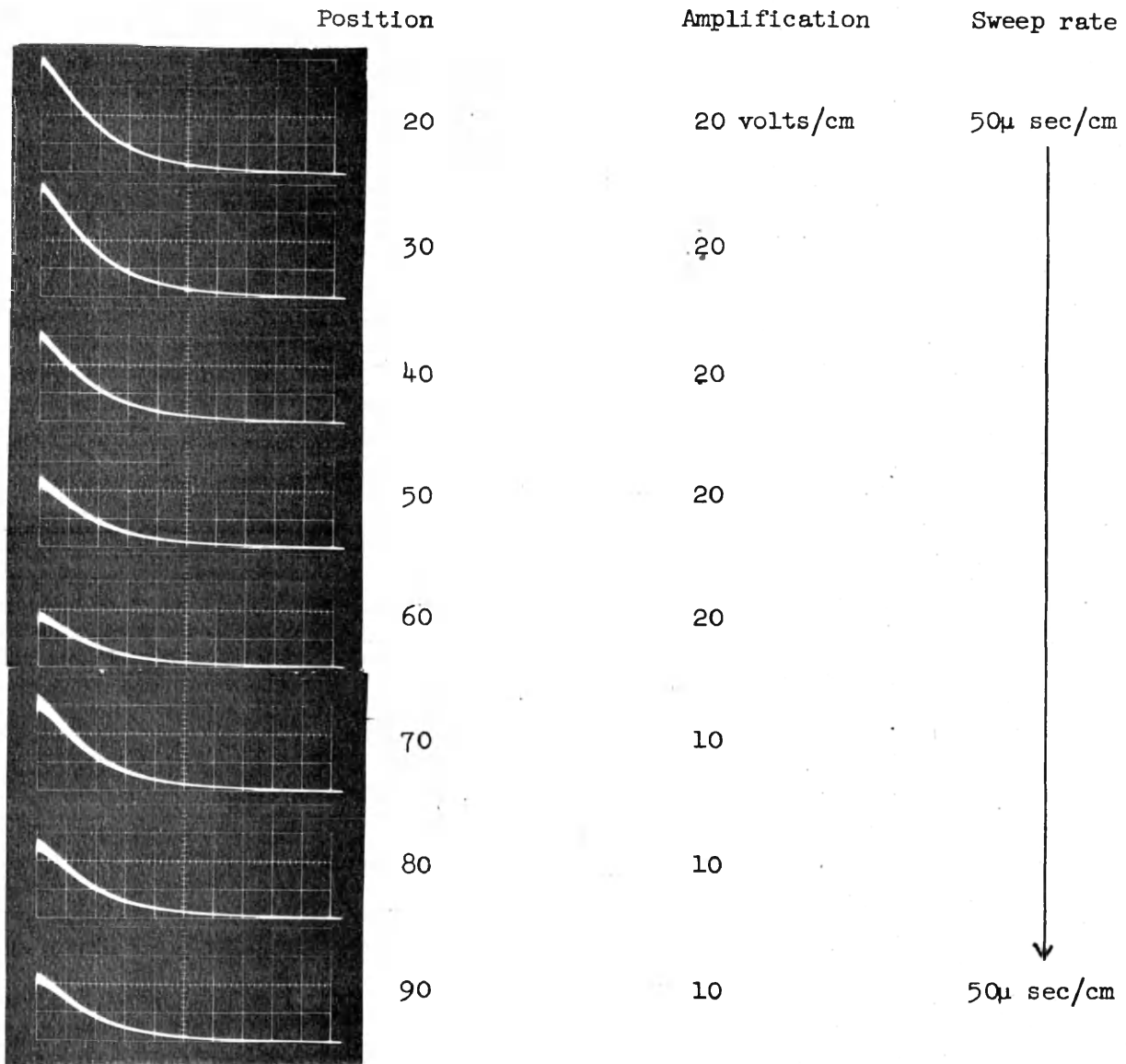


Figure 14.- Light decay as a function of distance from the accelerator.
Helium at a pressure of 5 μ Hg.

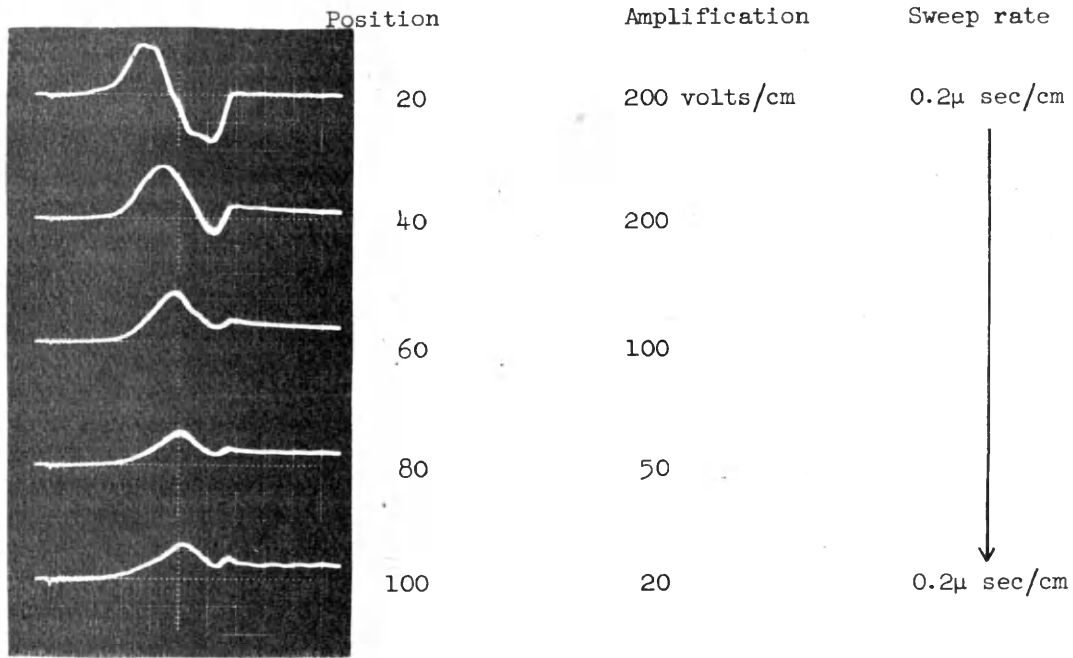


Figure 15.- Inductive probe signal decay as a function of distance from the accelerator. Air at a pressure of 5μ Hg.

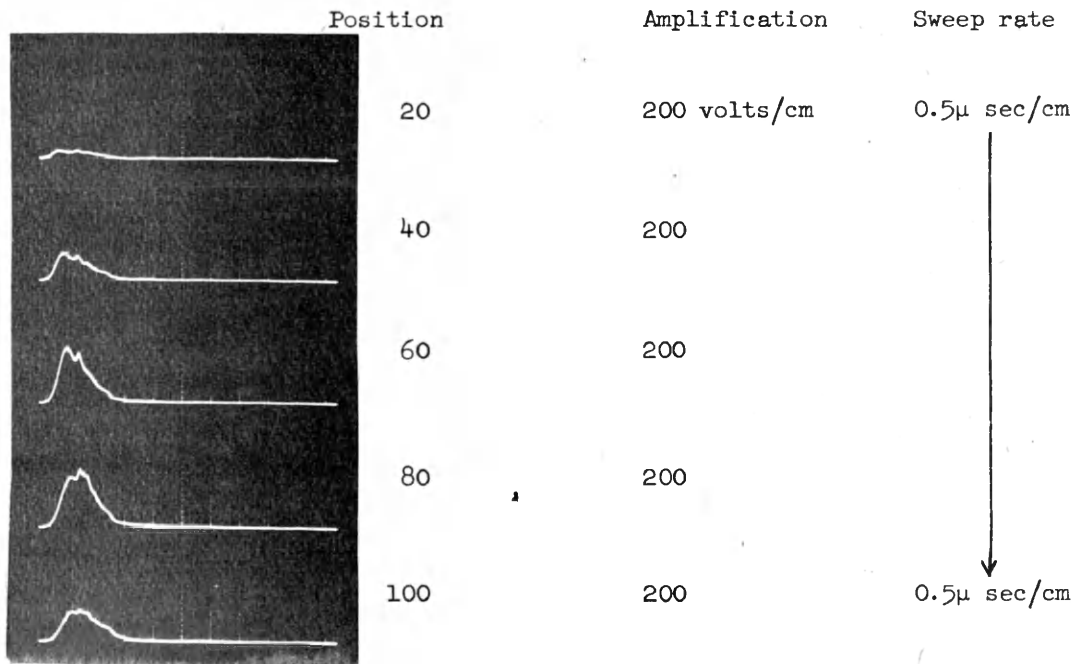


Figure 16.- Inductive probe signal decay as a function of distance from the accelerator. Helium at a pressure of 5μ Hg.

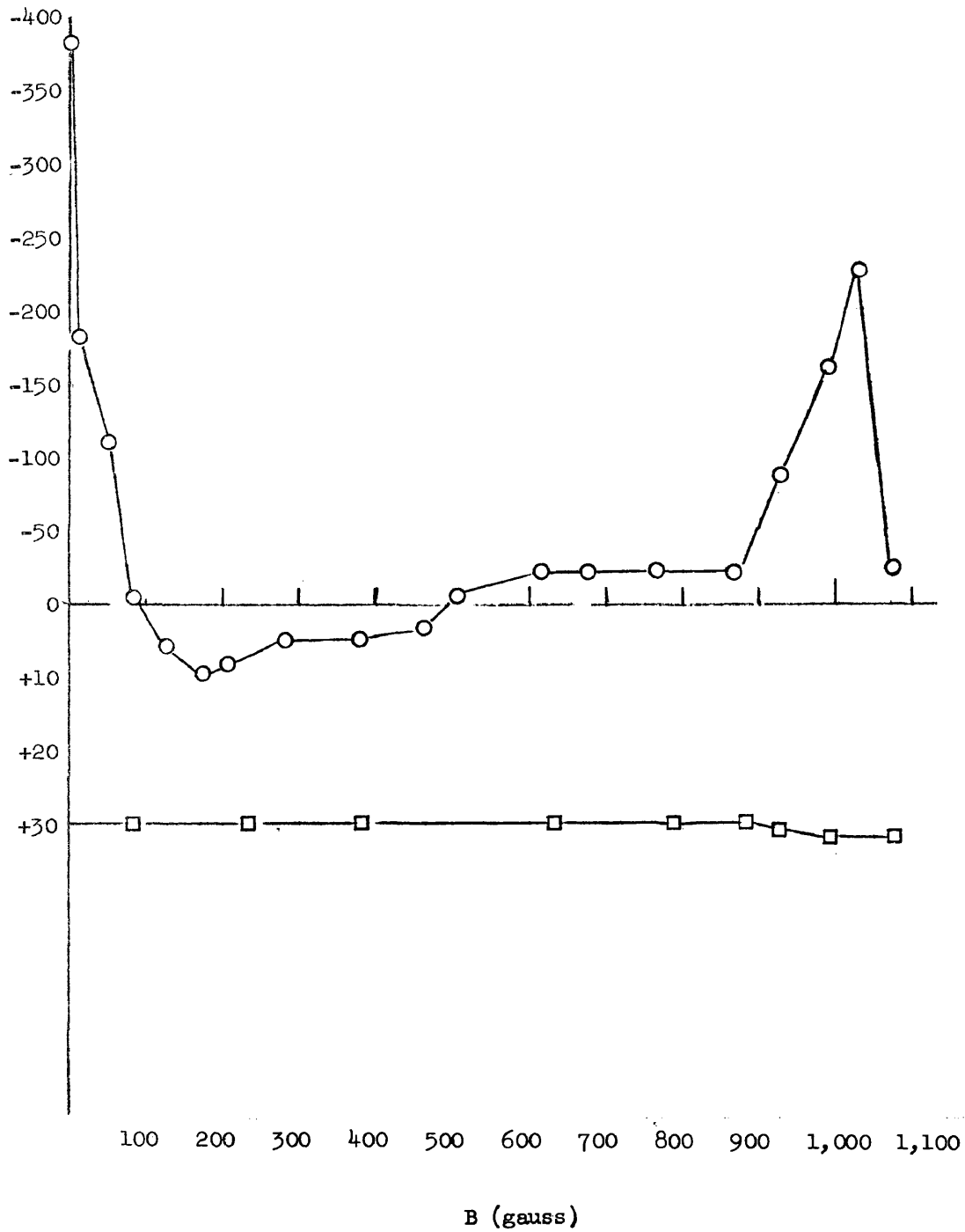


Figure 17.-- Air. (Upper) electron-ion difference current in microamps as a function of magnetic field, (lower) relative light outputs corresponding to currents above.

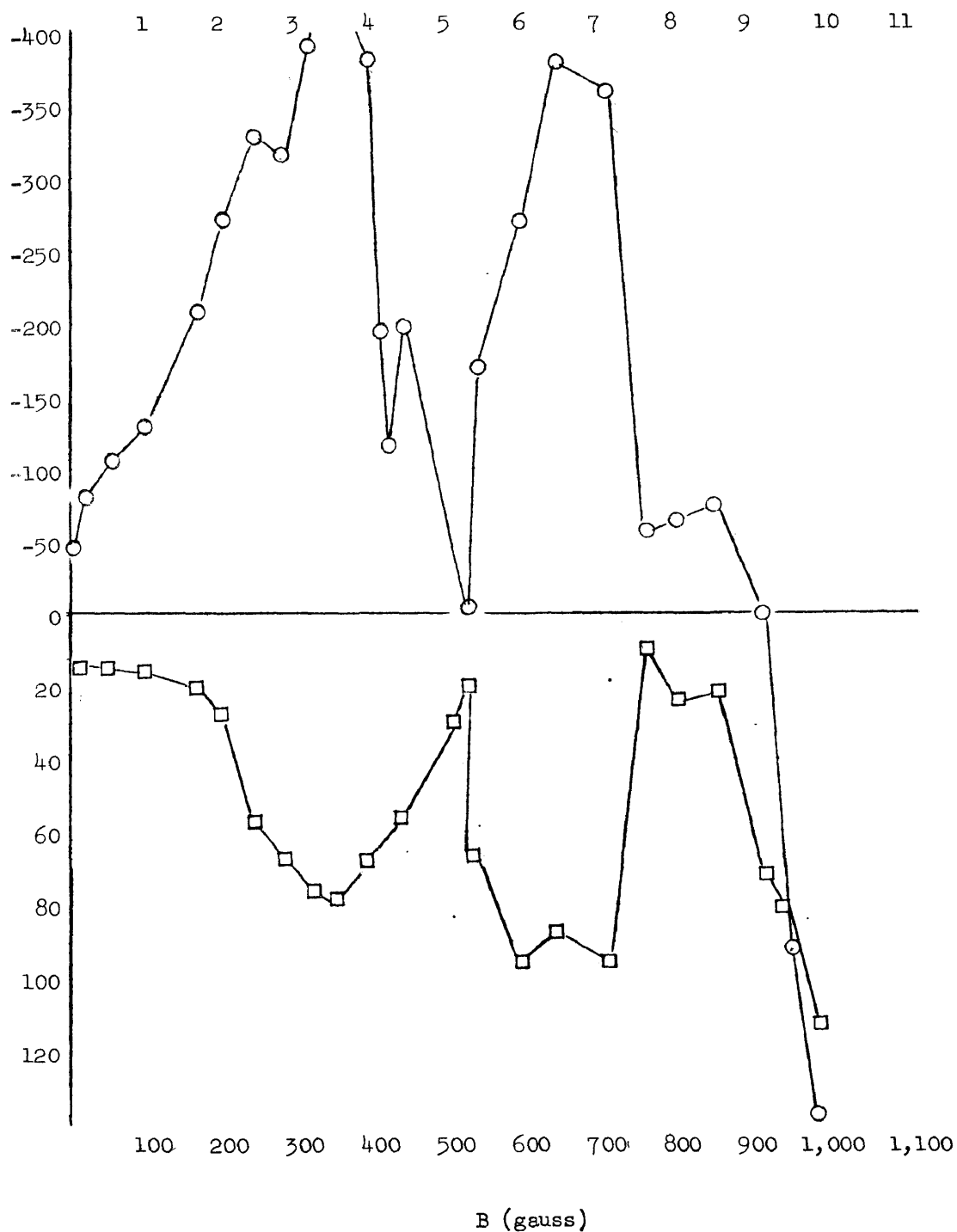


Figure 18.- Helium. (Upper) electron-ion difference current in microamps as a function of the magnetic field, (lower) outputs corresponding to currents above.

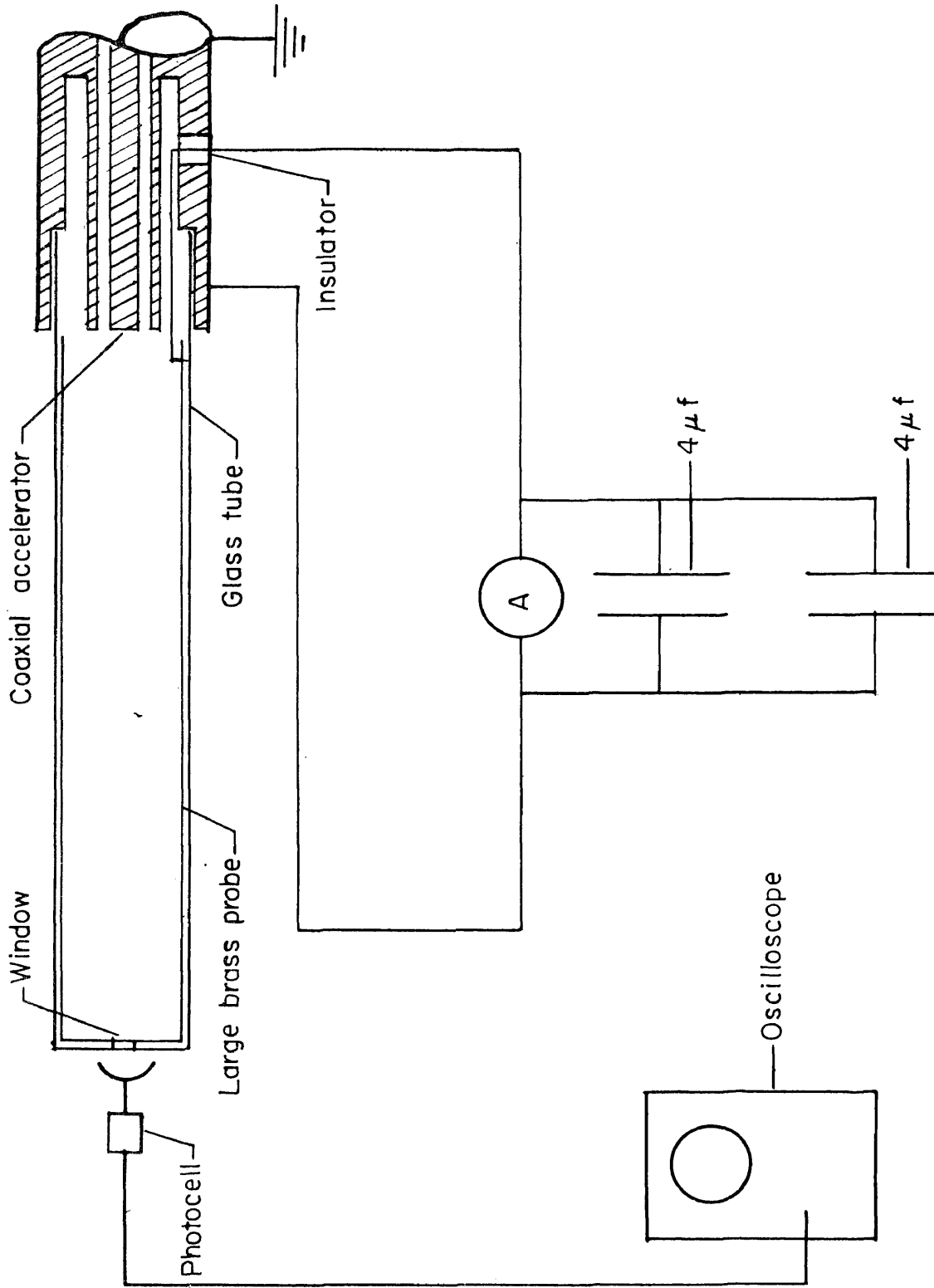


Figure 19.- Schematic of experimental setup to make simultaneous light output and current output measurements.

BIBLIOGRAPHY

1. Weibel, Erich S.: Confinement of a Plasma Column by Radiation Pressure. The Plasma in a Magnetic Field, edited by Rolf K. M. Landshoff, Stanford University Press, 1958.
2. Brown, Sanborn C.: Basic Data of Plasma Physics. Special Technical Report No. 2 of the M.I.T. Research Laboratory of Electronics. August 17, 1959.
3. Brown, Sanborn C.: High Frequency Gas-Discharge Breakdown. Technical Report No. 301. M.I.T. Research Laboratory of Electronics. July 25, 1955.
4. Hess, R. V., and Thom, K: Plasma Acceleration by Guided Microwaves. NASA TR, 1959.
5. Whitmer, R. F.: Principles of Microwave Interactions With Ionized Media. Sylvania, Technical Report MPL-M1, 1958.
6. Spitzer, Lyman, Jr.: Physics of Fully Ionized Gases. Interscience Tracts on Physics and Astronomy, 1956.

APPENDICES

APPENDIX A

DERIVATION OF THE EFFECTIVE DIELECTRIC CONSTANT FOR A
PLASMA INTERACTING WITH AN ELECTROMAGNETIC WAVE AND
A UNIFORM MAGNETIC FIELD

List of symbols used in these equations

- m mass of electron
- n number of electrons
- ν electron-neutral molecule collision frequency
- ω microwave radian frequency
- ω_c electron cyclotron frequency
- ω_p plasma frequency
- ϵ_0 free space dielectric constant
- ϵ effective dielectric constant

In comparing the Maxwell equation for fields depending on time as e^{-ikt}

$$\nabla \times H = \frac{\partial D}{\partial t} + J$$

and the corresponding equation in free space

$$\nabla \times H = -i\omega \epsilon_0 E$$

we can obtain an expression for the effective dielectric constant of a plasma. Only the electron oscillations in the high frequency fields are considered because the oscillations are too rapid for the heavy ions to follow.

Considering the Lorentz force equation with the collision frequency being introduced as a damping term and taking the magnetic field to be in the Z direction only (5)

$$m \frac{dJ}{dt} + m\nu J = ne^2 (E + V \times B_z) \quad (1)$$

Assuming the field variables to have the time dependence $e^{-i\omega t}$

$$-i\omega J + \nu J = \frac{ne^2}{m} E + \frac{ne^2}{m} (V \times B_z) \quad (2)$$

$$(\nu - i\omega)J = \epsilon_0 \omega_p^2 E + \frac{e}{m}(J \times B_z)$$

$$(\nu - i\omega)J = \epsilon_0 \omega_p^2 E + \frac{e}{m} \begin{vmatrix} 1 & j & k \\ J_x & J_y & J_z \\ 0 & 0 & B_z \end{vmatrix} \quad (3)$$

$$(\nu - i\omega)J_x = \epsilon_0 \omega_p^2 E_x + \frac{e}{m} J_y B_z$$

$$J_x = \frac{\omega_p^2}{(\nu - i\omega)} E_x + \frac{\omega_c}{(\nu - i\omega)} J_y \quad (4)$$

$$(\nu - i\omega)J_y = \epsilon_0 \omega_p^2 E_y - \frac{e}{m} J_x B_z$$

$$J_y = \epsilon_0 \frac{\omega_p^2}{(\nu - i\omega)} E_y - \frac{\omega_c}{(\nu - i\omega)} J_x \quad (5)$$

$$(\nu - i\omega)J_z = \epsilon_0 \omega_p^2 E_z$$

$$J_z = \epsilon_0 \frac{\omega_p^2}{(\nu - i\omega)} E_z \quad (6)$$

Substituting equation (5) into equation (4)

$$J_x = \epsilon_0 \frac{\omega_p^2}{(\nu - i\omega)} E_x + \frac{\omega_c}{(\nu - i\omega)} \left[\epsilon_0 \frac{\omega_p^2}{(\nu - i\omega)} E_y - \frac{\omega_c}{(\nu - i\omega)} J_x \right]$$

$$J_x = \epsilon_0 \frac{\omega_p^2}{(\nu - i\omega)} E_x + \epsilon_0 \frac{\omega_c \omega_p^2}{(\nu - i\omega)^2} E_y - \frac{\omega_c^2}{(\nu - i\omega)^2} J_x$$

$$J_x \left[1 + \frac{\omega_c^2}{(\nu - i\omega)^2} \right] = \epsilon_0 \frac{\omega_p^2}{\nu - i\omega} \left[E_x + \frac{\omega_c}{\nu - i\omega} E_y \right]$$

$$\left[\frac{(\nu - i\omega)^2 + \omega_c^2}{(\nu - i\omega)^2} \right] J_x = \epsilon_0 \frac{\omega_p^2}{\nu - i\omega} \left[E_x + \frac{\omega_c}{\nu - i\omega} E_y \right]$$

$$J_x = \epsilon_0 \frac{(\nu - i\omega)\omega_p^2}{(\nu - i\omega)^2 + \omega_c^2} \left[E_x + \frac{\omega_c}{\nu - i\omega} E_y \right]$$

$$J_x = \frac{\epsilon_0 \omega_p^2}{(\nu - i\omega)^2 + \omega_c^2} \left[(\nu - i\omega) E_x + \omega_c E_y \right] \quad (7)$$

Putting this value of J_x back into Maxwell's equations

$$\nabla \times H = \frac{\partial D}{\partial t} + J \quad (8)$$

$$\nabla \times H = \frac{\partial(\epsilon_0 E)}{\partial t} + J = -i\omega \epsilon_0 E + J$$

$$(\nabla \times H)_x = i\omega \epsilon_0 E_x + J_x$$

$$\begin{aligned}
 &= -i\omega\epsilon_0 E_x + \frac{\epsilon_0 \omega_p^2}{(\nu - i\omega)^2 + \omega_c^2} \left[(\nu - i\omega) E_x + \omega_c E_y \right] \\
 (\nabla \times H)_x &= \epsilon_0 \left[\left(-i\omega + \frac{\omega_p^2 (\nu - i\omega)}{(\nu - i\omega)^2 + \omega_c^2} \right) E_x + \left(\frac{\omega_p^2 \omega_c}{(\nu - i\omega)^2 + \omega_c^2} \right) E_y \right] \quad (9)
 \end{aligned}$$

Repeating the same procedure for the y component

$$\begin{aligned}
 J_y &= \epsilon_0 \frac{\omega_p^2}{(\nu - i\omega)} E_y - \frac{\omega_c}{(\nu - i\omega)} J_x = \epsilon_0 \frac{\omega_p^2}{(\nu - i\omega)} E_y - \frac{\omega_c}{(\nu - i\omega)} \left[\epsilon_0 \frac{\omega_p^2}{(\nu - i\omega)} E_x \right. \\
 &\quad \left. + \frac{\omega_c}{(\nu - i\omega)} J_y \right] J_y \left[1 + \frac{\omega_c^2}{(\nu - i\omega)^2} \right] = \frac{\epsilon_0 \omega_p^2}{\nu - i\omega} E_x - \frac{\epsilon_0 \omega_c \omega_p^2}{(\nu - i\omega)^2} E_x \\
 J_y &= \frac{(\nu - i\omega)^2}{(\nu - i\omega)^2 + \omega_c^2} \left[\frac{\epsilon_0 \omega_p^2}{\nu - i\omega} E_y - \epsilon_0 \frac{\omega_c \omega_p^2}{(\nu - i\omega)^2} E_x \right] \\
 &= - \frac{\epsilon_0 \omega_c \omega_p^2}{(\nu - i\omega)^2 + \omega_c^2} E_x + \frac{\epsilon_0 \omega_p^2 (\nu - i\omega)}{(\nu - i\omega)^2 + \omega_c^2} E_y \\
 J_y &= \frac{\epsilon_0 \omega_p^2}{(\nu - i\omega)^2 + \omega_c^2} \left[-\omega_c E_x + (\nu - i\omega) E_y \right] \quad (10)
 \end{aligned}$$

$$\begin{aligned}
 (\nabla \times H)_y &= -i\omega\epsilon_0 E_y + J_y \\
 &= -i\omega\epsilon_0 E_y + \frac{\epsilon_0 \omega_p^2}{(\nu - i\omega)^2 + \omega_c^2} \left[-\omega_c E_x + (\nu - i\omega) E_y \right]
 \end{aligned}$$

$$(\nabla \times H)_y = \epsilon_0 \left[\frac{\omega_c \omega_p^2}{(\nu - i\omega)^2 + \omega_c^2} E_x + \left(-i\omega + \frac{\omega_p^2 (\nu - i\omega)}{(\nu - i\omega)^2 + \omega_c^2} \right) E_y \right] \quad (11)$$

Since the magnetic field is parallel to the z axis, it has no effect in the z direction

$$J_z = \epsilon_0 \frac{\omega_p^2}{(\nu - i\omega)} E_z \quad (12)$$

$$(\nabla \times H)_z = -i\omega \epsilon_0 E_z + \frac{\omega_p^2}{(\nu - i\omega)} E_z$$

$$(\nabla \times H)_z = \epsilon_0 \left[-i\omega + \frac{\omega_p^2}{(\nu - i\omega)} \right] E_z \quad (13)$$

$$\left. \begin{aligned} \frac{1}{\epsilon_0} (\nabla \times H)_x &= \left[-i\omega + \frac{\omega_p^2 (\nu - i\omega)}{(\nu - i\omega)^2 + \omega_c^2} \right] E_x + \left[\frac{\omega_p^2 \omega_c}{(\nu - i\omega)^2 + \omega_c^2} \right] E_y \\ \frac{1}{\epsilon_0} (\nabla \times H)_y &= \left[\frac{\omega_p^2 \omega_c}{(\nu - i\omega)^2 + \omega_c^2} \right] E_x + \left[-i\omega + \frac{\omega_p^2 (\nu - i\omega)}{(\nu - i\omega)^2 + \omega_c^2} \right] E_y \\ \frac{1}{\epsilon_0} (\nabla \times H)_z &= \left[-i\omega + \frac{\omega_p^2}{(\nu - i\omega)} \right] E_z \end{aligned} \right\} \quad (14)$$

$$\left. \begin{aligned} (\nabla \times H)_x &= -i\omega \left[1 + \frac{\frac{\omega_p^2}{\omega} (\nu - i\omega) i}{(\nu - i\omega)^2 + \omega_c^2} \right] \epsilon_0 E_x - \left[\frac{i\omega_p^2 \omega_c \left(\frac{1}{\omega}\right)}{(\nu - i\omega)^2 + \omega_c^2} \right] \epsilon_0 E_y \\ (\nabla \times H)_y &= -i\omega \left[\frac{-i\omega_p^2 \omega_c \left(\frac{1}{\omega}\right)}{(\nu - i\omega)^2 + \omega_c^2} \right] \epsilon_0 E_x - i\omega \left[1 + \frac{\frac{\omega_p^2}{\omega} (\nu - i\omega) i}{(\nu - i\omega)^2 + \omega_c^2} \right] \epsilon_0 E_y \\ (\nabla \times H)_z &= -i\omega \left[1 + \frac{i\omega_p^2}{\omega(\nu - i\omega)} \right] \epsilon_0 E_z \end{aligned} \right\} \quad (15)$$

if we let

$$\epsilon_{11} = \left[1 + \frac{\omega_p^2}{\omega} \frac{(v - i\omega)i}{(v - i\omega)^2 + \omega_c^2} \right] = 1 - \omega_p^2 \frac{\left[(\omega^2 - \omega_c^2 + v^2) - i\left(\frac{v}{\omega}\right)(\omega^2 + \omega_c^2 + v^2) \right]}{\left[(\omega + \omega_c)^2 + v^2 \right] \left[(\omega - \omega_c)^2 + v^2 \right]}$$

$$\epsilon_{12} = \frac{\left[i\omega_c \omega_p^2 \left(\frac{1}{\omega}\right) \right]}{\left[(v - i\omega)^2 + \omega_c^2 \right]} = \omega_p^2 \omega_c \frac{\left[\left(\frac{1}{\omega}\right)(\omega_c^2 - \omega^2 + v^2) + 2iv \right]}{\left[(\omega + \omega_c)^2 + v^2 \right] \left[(\omega - \omega_c)^2 + v^2 \right]}$$

$$\epsilon_{33} = \left[1 + \frac{i\omega_p^2}{\omega(v - i\omega)} \right] = 1 - \omega_p^2 \frac{\left[1 - i\left(\frac{v}{\omega}\right) \right]}{\omega^2 + v^2}$$

Then

$$\nabla \times \mathbf{H} = -i\omega \begin{vmatrix} \epsilon_{11} & i\epsilon_{12} & 0 \\ -i\epsilon_{12} & \epsilon_{11} & 0 \\ 0 & 0 & \epsilon_{33} \end{vmatrix} \epsilon_0 \mathbf{E} \quad (16)$$

and the effective dielectric constant is

$$\epsilon = \begin{vmatrix} \epsilon_{11} & i\epsilon_{12} & 0 \\ -i\epsilon_{12} & \epsilon_{11} & 0 \\ 0 & 0 & \epsilon_{33} \end{vmatrix} \epsilon_0 \quad (17)$$

APPENDIX B

LIST OF EQUIPMENT

Microwave equipment

Radar transmitter	SCR-584
Magnetron	Type 2J31
Isolator	Microwave Associates Model 172
E-H plane tuner	Waveline, Type 260
Waveguide sections	Various manufacturers

Pulse equipment

Pulse generator	Hewlett Packard Model 212-A
Oscilloscope	Tektronix Type 545-A
Oscilloscope plug-in	Tektronix Type L
Time delay generator	Rutherford Model A-2

Vacuum equipment

Diffusion pump	C.E.C. Type MCF-300
Mechanical pump	Welch Duo Seal
Ionization gage control	C.V.C. Phillips PHG-09
Ionization gage tube	C.V.C. Phillips Phg-06
Thermocouple gage control	Hastings Type GV
Thermocouple gage tube	Hastings Type DV3M

Miscellaneous

Oscillograph camera	Dumont Type 302
Photocell	RCA Type 1P21
Photocell power supply	M.J.E. Corp. Type CS-51H34
D.C. power supply	G.E. Type MPC 7500A a 600V

ACKNOWLEDGEMENTS

The author wishes to express his appreciation to the National Aeronautics and Space Administration for the opportunity to use material in this thesis which was obtained from a research project conducted at their Langley laboratory.

He also wishes to thank Dr. Siegfried Vogel as the project leader for his suggestions in carrying out the experiments, and Dr. Frederic R. Crownfield, Jr., Dr. Donald E. McLennan, and Dr. James D. Lawrence, Jr. for their advice and assistance in preparing this thesis.